J. Fluid Mech. (2007), *vol.* 572, *pp.* 121–144.
doi:10.1017/S0022112006003430 Printed in the United Kingdom

Low-pressure flashing mechanisms in iso-octane liquid jets

By M. M. VIEIRA AND J. R. SIMÕES-MOREIRA

SISEA – Alternative Energy Systems Laboratory, Mechanical Engineering Department at Escola Politécnica, Universidade de São Paulo, São Paulo, SP – Brazil
jrsimoes@usp.br

(Received 14 October 2005 and in revised form 26 June 2006)

This paper examines a flashing liquid regime that takes place at very high ratios of injection to discharge pressures in flow restrictions. Typically, the flashing phenomenon has been observed in laboratory experiments where a liquid flows through a short nozzle into a low-pressure chamber at a pressure value considerably lower than the liquid saturation pressure at the injection temperature. By using two visualization techniques, the schlieren and the back-lighting methods, it was possible to identify some compressible phenomena associated with the liquid flashing process from the nozzle exit section. The schlieren method was used to capture the image of a shock-wave structure surrounding a liquid core from which the phase change takes place, and the optical technique allowed us to observe the central liquid core itself. The work corroborates previous physical descriptions of flashing liquid jets to explain an observed choking behaviour as well as the presence of shock waves. According to the present analysis, flashing takes place on the surface of the liquid core through an evaporation wave process, which results from a sudden liquid evaporation in a discontinuous process. Downstream of the evaporation discontinuity, the two-phase flow reaches very high velocities, up to the local sonic speed that typically occurs at high expansion conditions, as inferred from experiments and the physical model. That sonic state is also a point of maximum mass flow rate and it is known as the Chapman–Jouguet condition. The freshly sonic two-phase flow expands freely to increasing supersonic velocities and eventually terminates the expansion process through a shock-wave structure. This paper presents experimental results at several test conditions with iso-octane.

1. Introduction

The expansion process of a liquid flowing through a constriction such as an orifice or a short nozzle may take the liquid into the saturation condition for certain combinations of pressure drop and thermodynamic properties of the fluid, which would trigger the phase-change process as dictated by equilibrium thermodynamics. However, in some situations, the expansion process may proceed further, with the liquid reaching a superheated or metastable thermodynamic state without any phase transition. This situation sets the condition for a vigorous adiabatic phase change through a discontinuity process called an evaporation wave (Simões-Moreira & Shepherd 1999). Evaporation waves are adiabatic phase-change processes in which a superheated liquid undergoes a phase change in a discrete liquid two-phase interface in

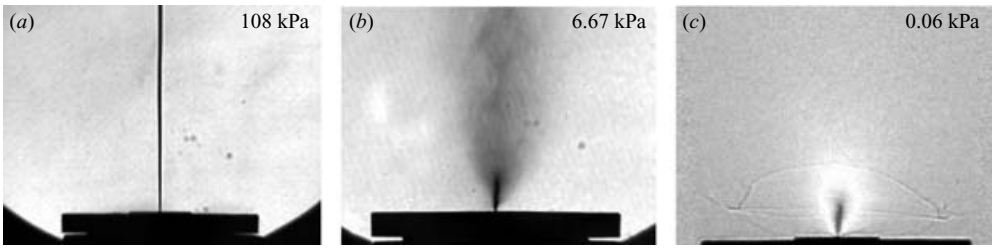

FIGURE 1. Test series at nominal injection values $P_0 = 250\,\text{kPa}$ and $T_0 = 76\,^\circ\text{C}$: from (*a*) to (*c*), backpressure decreases ($P_\infty = 108$, 6.67 and 0.06 kPa, respectively). (*a*) A continuous jet. (*b*) The jet undergoes evaporation as it shatters. (*c*) The liquid jet is surrounded by a shock-wave structure.

a similar fashion to the deflagration phenomenon in a combusting gas. Evaporation wave theory plays an important role in flashing liquids, as studied in this work, as it explains some of the main features directly observed as well as some others inferred from the experiments. In a broader sense, the phase change associated with a depressurization process is generally known as flashing. This paper examines the physics associated with certain liquid flashing regimes where a liquid jet is subjected to large pressure drops that instigate compressible phenomena such as shock wave and flow choking, which can be explained within the evaporation wave theory framework. The sequence of still pictures in figure 1 was taken from experiments carried out with liquid iso-octane (C_8H_{18}) jets issuing from a small conical converging nozzle into a low-pressure chamber, and reveal some important features of flashing jets. If there is no evaporation, the flow of the liquid jet from the nozzle exit section remains intact and follows a straight path. On the other hand, if evaporation takes place, which occurs at backpressures lower than the vapour pressure at the initial testing temperature, breakup points associated with bubble growth due to nucleation are visible. As seen in the figure, on decreasing the backpressure, the liquid jet shatters giving rise to a cloud of droplets, indicating a large number of nucleation sites and rapid bubble growth. On decreasing the backpressure further, it is possible to see the liquid jet (a liquid core) emerging from the nozzle, with a cloud of droplets, and a shock-wave structure enveloping the liquid core. In this situation, at very low backpressures, it has been inferred from photographs (Reitz 1990; Kurschat, Chaves & Meier 1992; Athans 1995; Simões-Moreira, Vieira & Angelo 2002) that no phase transition or nucleation sites are observed in the liquid jet at the exit plane of the nozzle. Still pictures taken using different photographic techniques (Reitz 1990; Kurschat *et al.* 1992; Athans 1995; Simões-Moreira *et al.* 2002; Vieira 2005; Vieira & Simões-Moreira 2006) at a high shutter speed show that the jet emerging from the nozzle remains in the liquid phase. With the usual assumption of incompressible flow for the liquid portion within the nozzle, the incompressible version of Bernoulli's equation along with the measured mass flow rate implies that the emerging liquid must be at a highly superheated or metastable state at the nozzle exit section, i.e. the liquid state is deep into the metastable region. This description is valid for a low chamber pressure, i.e. a backpressure value below the saturation pressure corresponding to the initial injection temperature. The fact that the jet emerges in the liquid phase is striking, because laboratory experiments (Simões-Moreira *et al.* 2002; Vieira & Simões-Moreira 2004) have shown that there is flow choking behaviour as the mass flow rate becomes constant and insensitive to pressure reduction below some backpressure threshold. In addition, by using two different visualization techniques,

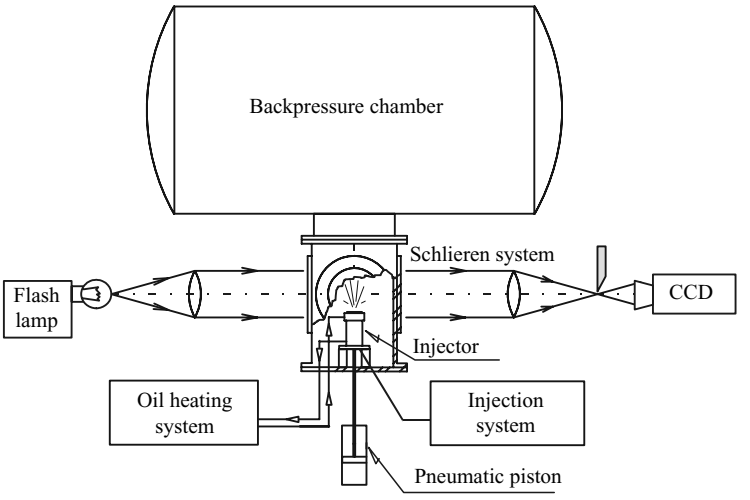

FIGURE 2. General scheme of the test rig.

the schlieren and the back-lighting methods, it was possible to identify compressible phenomena associated with the flashing process. The schlieren method was used to capture the image of a shock-structure wave surrounding the liquid core, and the optical technique allowed us to observe the central liquid core. This corroborates a physical description of flashing liquid jets that explains the choking behaviour and the presence of shock waves using the concept of evaporation waves. This paper presents additional experimental results at several experimental conditions with iso-octane and is a corroborative and extended analysis of Simões-Moreira *et al.* (2002).

2. Apparatus and experimental procedure

The test rig (figure 2) allowed us to control the injection pressure and temperature of the test liquid as well as the backpressure. The test liquid, iso-octane, was injected through a nozzle into a low-pressure chamber and the jet exit region was imaged by either the schlieren, or the back-lighting optical set-up, or both. Further operational details, details of instrumentation, as well as more complete schematics can be found in Simões-Moreira *et al.* (2002) and Vieira (2005).

The flashing jet discharged into a low-pressure chamber of approximately 0.440 m^3, which was large enough to carry out up to two tests with 8 cm^3 of liquid without any significant pressure rise in the chamber for many of the experiments during a time interval of approximately 4 s.

The main part of the nozzle was formed by a conical converging nozzle made of regular machined carbon steel having an exit section of 0.31 ± 0.01 mm, a rounded entrance diameter of 3 mm, and a total length of 8 mm. Oil flowing around the nozzle and the test liquid cell provided heating to the desired injection temperature. A pneumatic piston (figure 2) opened and closed the nozzle quickly. The injection system was intended to maintain a constant liquid pressure during an injection cycle, as well as to determine the injected liquid volume. The injection temperature was monitored by a thermocouple (type T, *awg* 30) positioned a few millimetres upstream of the nozzle entrance section and the pressure measured was using a pressure transducer (Kulite – xte-190-250-A). Temperature and pressure signals were digitized using a regular 12-bit data acquisition system. The pressure transducer signal confirmed that

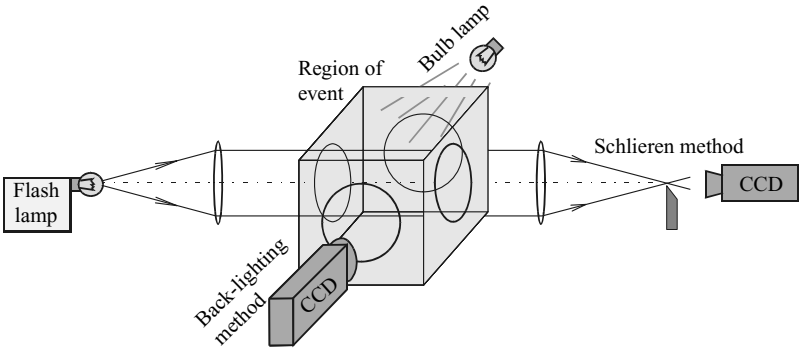

FIGURE 3. Schematic of the visualization systems showing both the 'schlieren' and the 'back-lighting' methods.

a steady-state condition was achieved within a few milliseconds of the nozzle opening (refer to figure 8 in Simões-Moreira *et al.* 2002).

A visualization system was used based on the classical schlieren method in the 'Z' configuration. Parabolic mirrors were used to obtain a parallel light beam covering a 10 cm diameter circular region. A monochromatic CCD camera (a camera with Charged Coupled Device, Coastar model CV-M50) imaged the region of interest and obtained at a regular rate of 30 per second. The light source was a flash lamp (EG&G model LS-1130) giving an overall exposure time as low as 2 μs, providing clear images. An image acquisition system (Data Translator model DT-3152) captured the CCD images. Between five and nine frames were acquired during a typical injection process, but the first frame was taken just before the event started for subsequent image filtering purposes and the remaining frames were then obtained. A subtraction-type mathematical filter was later used to obtain sharper images. The second visualization system is based on the method of back-lighting and uses an identical CCD camera (figure 3).

The nozzle discharge coefficient, C_D, was obtained experimentally, and the final curve (data fitting) is given by,

$$C_D = 0.9673 - 5.6682/\sqrt{Re}, \tag{1}$$

where Re is the Reynolds number based on the nozzle exit diameter, D. The uncertainties in the measurements were ± 1.8 kPa, ± 1.2°C, ± 0.06 kPa and ± 2 % for injection pressure, temperature, backpressure and mass flow rate.

3. Experimental results

3.1. *Importance of photographic techniques*

Figure 4(*a*) was taken using a regular photographic technique with a shutter speed of 1/60 s. In view of the high fluid velocities the image is blurred, and cannot resolve flow details of the phenomena present in a flashing liquid. Fluid paths are streaks emanating from a central core spreading into the low-pressure environment. It is difficult to conclude that any compressible phenomenon is present or to distinguish a flashing mechanism by using this photographic technique alone. Oza & Sinnamon (1983) were misled in their conclusions as they proposed a theory of an internal flashing boiling mechanism to explain flow choking based on regular still photography techniques. According to this, the phase-change process would be triggered within the

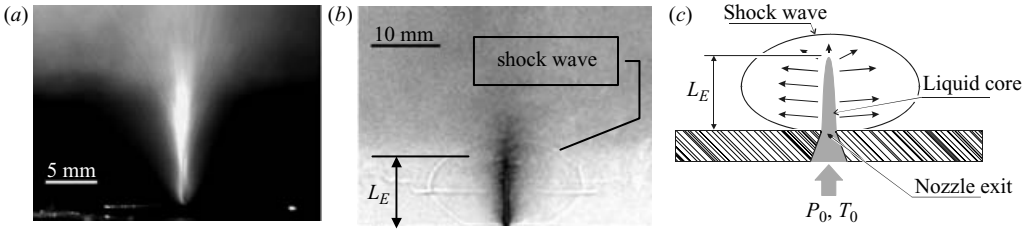

FIGURE 4. Photographs and schematics of the flashing liquid jet – flashing was triggered at or very near to the nozzle exit section. (*a*) Regular photograph (1/60 s) using back-lighting illumination technique; (*b*) schlieren photograph (2 μs); (*c*) schematics of the phenomenon stressing a central liquid core, the enveloping shock-wave structure, and the liquid core extinction length, L_E ($P_0 = 750.7$ kPa, $T_0 = 77.1\,^{\circ}$C and $P_\infty = 0.32$ kPa).

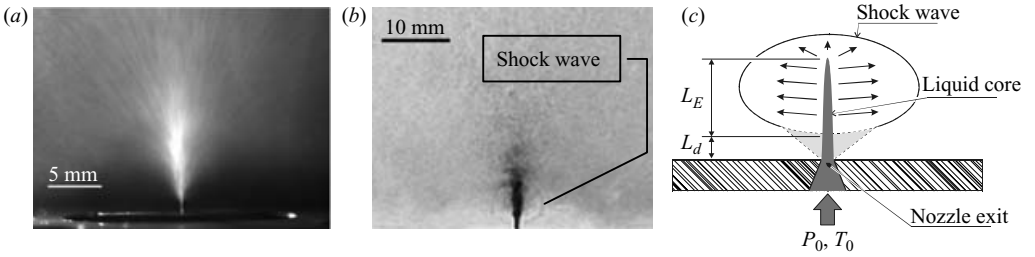

FIGURE 5. Photographs and schematics of the flashing liquid jet – flashing was triggered after some delay. (*a*) Regular photograph (1/60 s) using back-lighting illumination technique; (*b*) schlieren photograph (2 μs); (*c*) schematics of the phenomenon stressing a central liquid core, the enveloping shock-wave structure, the liquid core extinction length L_E and the length corresponding to some flashing start-up delay L_D ($P_0 = 122.1$ kPa, $T_0 = 56.4\,^{\circ}$C and $P_\infty = 0.45$ kPa).

nozzle, giving rise to an internal two-phase flow whose vapour compressibility would take the mixture to a choking condition. In a more detailed photographic study, Reitz (1990) showed that flashing actually took place away from the nozzle for the tested experimental conditions. Compressible phenomenon such as shock waves are captured well using the classical schlieren technique and for this reason it was also used in this study. Figure 4(*b*) shows a schlieren photograph taken at the same time as figure 4(*a*), i.e. both photographs refer to the same experiment. Also, figure 4(*b*) was taken at a 2 μs shutter speed, making it clear. A different phenomenon is discernible. The most important point is that a shock-wave structure is clearly seen surrounding a central liquid core. The presence of a shock-wave structure indicates that the flow was accelerated to supersonic condition, a phenomenon only detected previously by a few workers (Kurschat *et al.* 1992; Athans 1995; Simões-Moreira *et al.* 2002; Vieira 2005; Vieira & Simões-Moreira 2004, 2006). Figure 4(*c*) can be produced after analysing the schlieren photograph. The two-phase flow pathlines emanating from a liquid core are indicated, terminating in the shock wave.

3.2. *Phase change delay*

In most of the experiments carried out in this study, the onset of phase change was triggered at or very close to the nozzle exit section (figure 4*c*). However, in a few experiments at some experimental conditions, there was some phase change delay before flashing started. This is illustrated well by figures 5(*a*) and 5(*b*). In figure 5(*a*), a regular still picture (1/60 s) shows that the flashing phenomenon started at some

P_0 ± 1.8 (kPa)	T_0 ± 1.2 (°C)	P_∞ ± 0.06 (kPa)	P_σ $\pm 3\,\%$ (kPa)	R_P P_σ/P_∞ –	C_D ± 0.018 –	$\dot{m}$ $\pm 2\%$ ($g\,s^{-1}$)	P_1 (kPa)	$\Pi = (P_\sigma - P_1)/P_\sigma$ –	L_E/D –	Delay –
122.1	56.4	0.49	25.0	51.0	0.913	0.8447	4.2	0.832	20.10	Yes
122.7	75.2	0.14	48.9	349.0	0.917	0.8340	6.6	0.865	13.61	Yes
123.5	94.8	0.15	89.7	597.8	0.920	0.8022	14.7	0.836	7.46	Yes
249.0	56.9	0.08	25.5	318.4	0.922	1.2103	9.4	0.631	23.99	Yes
251.8	76.6	0.18	51.2	284.4	0.925	1.1872	18.4	0.641	20.42	Yes
250.5	94.7	9.93	88.8	8.9	0.927	1.1210	39.4	0.556	14.23	–
249.6	120.2	1.60	177.5	111.0	0.928	0.9456	94.7	0.467	10.05	–
257.1	130.9	0.48	229.8	478.7	0.926	0.8102	140.8	0.387	9.40	–
501.6	56.6	0.20	25.2	126.0	0.929	1.7455	15.9	0.369	37.28	Yes
497.6	76.9	0.11	51.7	470.0	0.932	1.6993	30.6	0.408	25.28	–
503.4	95.4	0.96	91.2	95.0	0.934	1.6528	53.6	0.412	18.48	–
503.3	120.6	0.26	179.3	689.7	0.936	1.4822	131.8	0.265	12.64	–
500.0	131.0	0.45	230.3	511.8	0.936	1.3757	175.1	0.240	11.67	–
502.1	162.1	0.55	448.9	816.1	0.933	0.9286	342.8	0.236	6.81	–
750.4	56.1	12.40	26.6	2.1	0.933	2.1471	21.7	0.183	46.68	–
752.5	77.0	0.54	51.9	96.1	0.936	2.0910	50.5	0.026	33.39	–
748.4	95.3	0.31	91.0	293.5	0.937	2.0112	89.9	0.012	24.64	–
753.2	121.1	0.20	181.5	907.7	0.939	1.8833	161.0	0.113	16.21	–
749.6	131.9	0.27	235.2	871.1	0.939	1.7599	224.6	0.045	14.26	–
749.2	161.8	0.48	446.2	929.6	0.939	1.3746	409.2	0.083	7.46	–
751.6	178.1	0.13	610.7	4697.8	0.936	0.9809	569.5	0.067	5.51	–

TABLE 1. Main experimental results. P_0 and T_0 are the injection pressure and temperature; P_∞ is the backpressure; P_σ and P_1 are the saturation pressure at T_0 and the metastable pressure; R_P is the ratio between saturation pressure and backpressure; C_D is the discharge coefficient; $\dot{m}$ is the mass flow rate; Π is the dimensionless degree of metastability and; L_E/D corresponds to the ratio between the liquid core extinction length and exit nozzle diameter. The last column indicates whether that specific run presented a phase change delay or not.

distance away from the nozzle exit section (L_d). The simultaneous schlieren picture (figure 5*b*) shows a shock-wave geometry slightly different from the previous ones as the shock-wave structure seems to fold itself around the central liquid core, unlike the shock-wave geometry seen in figure 4(*b*). Figure 5(*c*) is a sketch of this shock geometry. A striking point is that this delay was reproducible and consistently occurred in the low-temperature range. The main focus of the present work is the flashing conditions illustrated by the still pictures in figure 4; the phase-change delay remains to be elucidated and will not be examined here. The phase-change delay problem has already been studied by Lienhard & Day (1970). The main consequence of a phase-change delay is that the downstream boundary conditions are somewhat different from those without a delay. As it will be seen in the following sections, as the phase change takes place on the central liquid core, it opens up, expanding freely in all directions and reaching supersonic conditions. The high-speed two-phase flow expands supersonically until a shock wave is formed to match the pressure in the far field.

3.3. *Experimental data*

A set of selected data is presented in table 1. The first two columns show the injection pressure P_0 and temperature T_0, respectively. P_∞ is the low-pressure chamber pressure. The corresponding saturation pressure at the injection temperature is P_σ. The

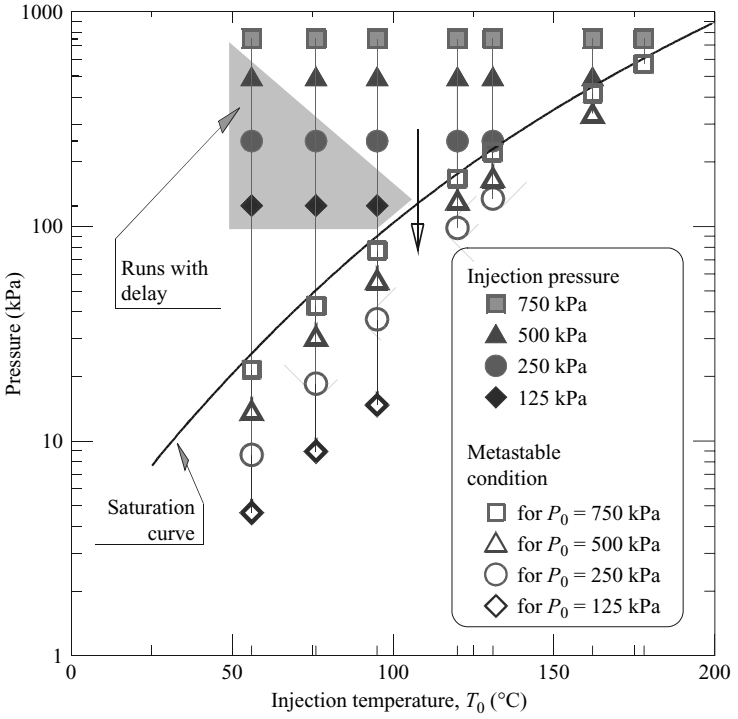

FIGURE 6. Pressure vs. temperature diagram showing the injection, the saturation, and the metastable pressures for the experimental data given in table 1. Expansion within the nozzle follows a near isothermal process.

parameter R_P is the pressure ratio between the saturation pressure, P_σ, taken at the injection temperature and the chamber pressure, P_∞, i.e. $R_P = P_\sigma / P_\infty$. The discharge coefficient, C_D, is given in the next column. The inferred metastable liquid pressure P_1 is shown next, which is the pressure at the nozzle exit section. The next column displays the measured mass flow rate, $\dot{m}$. A dimensionless degree-of-metastability parameter $\Pi = (P_\sigma - P_1)/P_\sigma$ is shown and L_E/D is the ratio between the extinction length and the nozzle exit diameter. Measured and calculated uncertainties are also indicated. The metastable pressure P_1 was not measured directly, but calculated from the orifice equation

$$P_1 = P_0 - \frac{\dot{m}^2 v}{2A^2 C_D^2}. \tag{2}$$

Where, v is the average between nozzle inlet and outlet liquid specific volumes, A is the nozzle exit cross-section, and the remaining magnitudes have been defined already. Finally, a yes indication in the last column points out that there was a phase delay for that specific run.

Figure 6 displays the relevant pressure and temperature data as well as the saturation curve for iso-octane. Injection conditions are those shown in solid symbols above the saturation curve. Each symbol type denotes one of the four injection pressures tested, namely, 125, 250, 500 and 750 kPa. The graph also shows the metastable pressure calculated according to (2). Numerical values corresponding to these data points are given in table 1. The shaded trapezoidal region delineates the

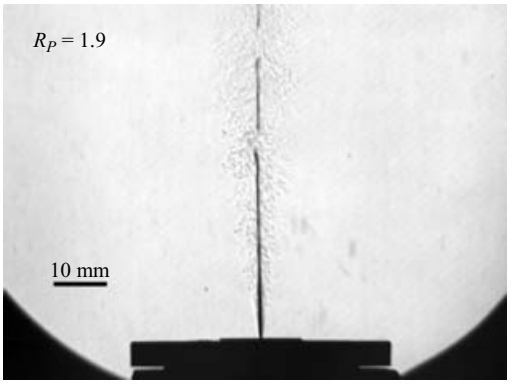

FIGURE 7. Liquid jet breakup by nucleation (injection conditions: $P_0 = 250.3$ kPa and $T_0 = 119.8\,^{\circ}$C), backpressure is $P_\infty = 89.9$ kPa which yields $R_P = 1.9$).

experiments in which the flashing delay was noticeable. The whole expansion process within the nozzle follows a near isothermal path as is usual for liquids, which explains why the injection, the saturation, and the metastable pressures are located on a nearly vertical line in this diagram. For a given temperature, the lower the injection pressure, the deeper the liquid enters into the metastable region.

4. Flashing associated phenomena

4.1. *Metastable liquid, choking and extinction length*

A systematic investigation was carried out in order to observe the influence of the injection temperature and pressure on the dynamic behaviour of the jet, its extinction length, and the flow choking conditions. To achieve that goal, a set of nominal injection pressures were tested, 125, 250, 500 and 750 kPa, which were combined with nominal injection temperatures of 56, 76, 95, 120, 131, 162 and 178 °C forming a test matrix covering a large range of data. Those values were chosen so that the non-dimensional pressure ratio, R_P, took nominal values of 0.5, 1, 2, 5, 10, 100, 200, 500, 1000 and 2000. R_P also provides a systematic way of checking the influence of the backpressure or chamber pressure on the overall behaviour of the liquid flashing jet. In figure 7 ($R_P \approx 2$), there is a continuous liquid jet disturbed by sporadic breakup points due to jet lengthwise bubble growth. Pressure ratios around unity and lower, yield a continuous liquid jet, which is not relevant to this work. As R_P increases from 5 to 10, easily accomplished by decreasing the backpressure, it is possible to see a partially shattering liquid jet (figure 8*a*) as a consequence of the vigorous evaporation process that is taking place. Also, a cloud of high-speed droplets is observed leaving from a central liquid core (figure 8*b*). At extreme conditions (R_p above 50 or 100 – depending on the testing temperature), the liquid jet assumes an axisymmetric shape, and shock waves are clearly seen (figure 9).

The schlieren image sequence of figure 9 corresponds to R_P values of 50, 100 and 500, which were set by decreasing the backpressure, keeping the injection temperature (56 °C) and pressure (500 kPa) constant. The major influence of the backpressure on the overall behaviour of the flashing liquid jet at these high pressure ratios is mostly related to the shock-wave main dimensions. As the backpressure decreases (R_P increases) the enveloping shock wave bulges each time providing a larger structure enclosing the central liquid core.

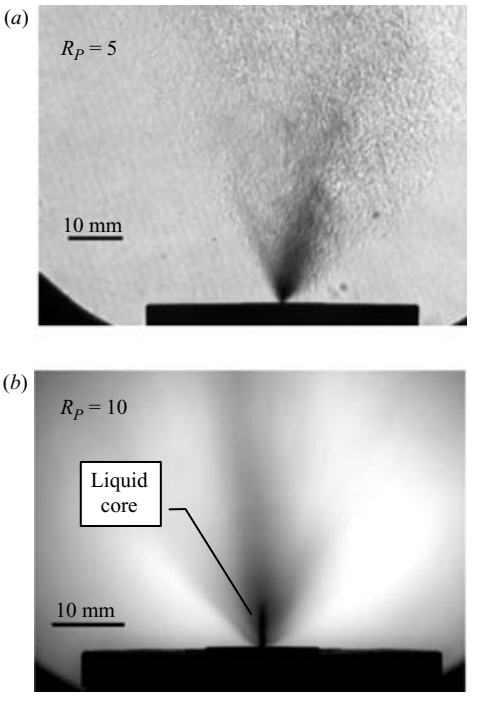

FIGURE 8. (*a*) A partially shattering liquid jet ($P_0 = 252.6$ kPa, $T_0 = 129.8\,^{\circ}$C, $P_\infty = 43.7$ kPa and $R_P = 5$); (*b*) a cloud of droplets leaving from a central liquid core ($P_0 = 501.9$ kPa, $T_0 = 95.4\,^{\circ}$C, $P_\infty = 9.2$ kPa and $R_P = 10$).

An important feature of flashing liquid jets is the mass flow rate behaviour. Figure 10 shows a typical result of the measured mass flow rate, $\dot{m}$, as a function of the pressure ratio P_∞/P_0 for four injection temperatures (76, 95, 120 and 130 °C) and an injection pressure of 250 kPa. Similar behaviour was found for other injection pressures. Analysing the curves in this figure from right to left shows that as the backpressure is decreased, at first there is no flashing because the backpressure is above the saturation pressure at the injection temperature. In this flow regime, the mass flow rate is calculated according to the orifice discharge formula, (2), where P_1 is replaced by P_∞ and, consequently, the mass flow rate is directly proportional to the square root of the pressure drop as is usual for incompressible single-phase fluids. As the backpressure is reduced further, a pressure ratio threshold is reached, from which the mass flow rate becomes backpressure-independent, taking constant values that depend on the injection pressure and temperature for a given fluid and nozzle geometry. An upper mass flow rate limit signifies that a choking condition has been reached. The choking flow behaviour corroborates the thermodynamic model presented in this paper as well as in previous studies (Simões-Moreira *et al.* 2002; Vieira & Simões-Moreira 2004; Angelo & Simões-Moreira 2004).

A parameter that is germane for characterizing the evaporation rate is the metastable liquid core extinction length, L_E, which is the length of the central liquid core measured from the nozzle exit plane to the point where the liquid core vanishes. An illustration of the extinction length is given in the bottom left-hand corner of figure 11. It is remarkable that its magnitude is reproducible in tests at the same conditions. Figure 11 displays the measured extinction length as a function of

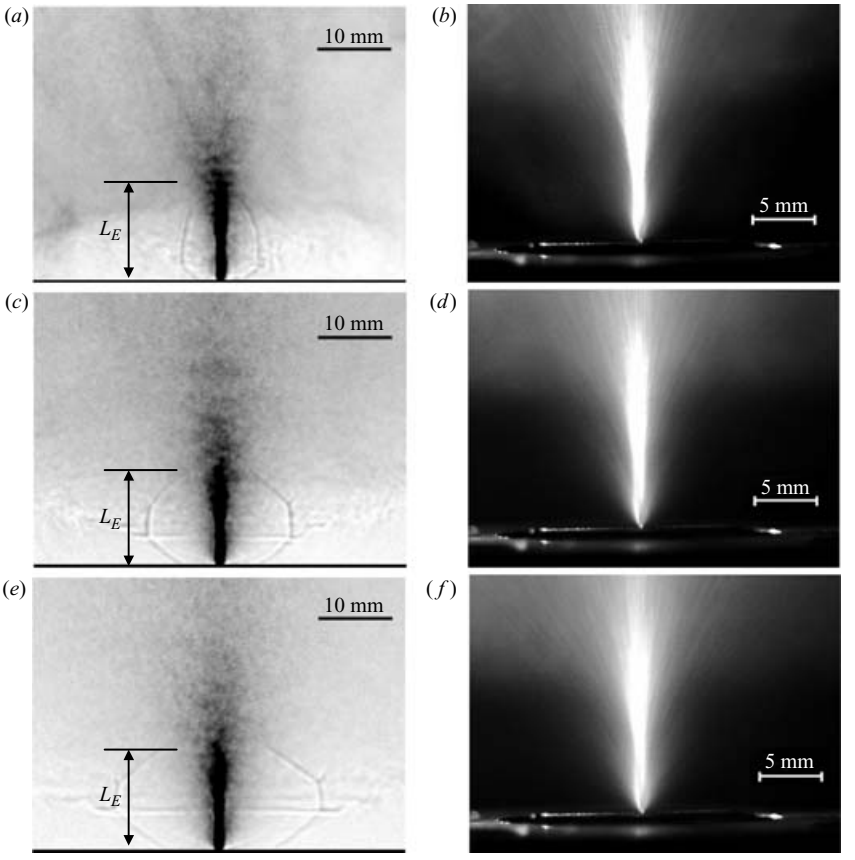

FIGURE 9. Sequence of images of jets with constant injection conditions ($P_0 = 500$ kPa and $T_0 = 56$ °C), for $R_P = 50$, 100 and 500, which correspond to backpressure set to 0.50, 0.31 and 0.12 kPa, respectively. (a, c, e) Schlieren arrangement; (b, d, f) corresponding back-lighting method.

the saturation-to-injection pressure ratio, for several injection pressures (125, 250, 500 and 750 kPa) as well as for some experimental data from Athans (1995). That figure shows that for a given injection pressure, the extinction length decreases significantly as the saturation pressure increases, which occurs for higher injection temperature, since the saturation pressure is temperature dependent. More precisely, the data trend indicates that there is an exponential functional dependence of L_E on the saturation-to-injection pressure ratio. Another set of experiments investigated whether there was a relationship between the extinction length and the backpressure. In order to verify this, both the injection pressure and temperature were kept constant and the backpressure was varied. The test results are presented in table 2, where the injection pressure, temperature, tested backpressure corresponding saturation and backpressure ratio, R_P, the mass flow rate, and the extinction length are shown. Those experiments confirm the previous assumption that the extinction length is not affected by the backpressure in this low pressure range. Consequently, a second important conclusion is that extinction length is independent of the backpressure up to a certain threshold value, which also comprises the choking flow region. Therefore, there exists a direct relationship between flow choking, mass flow rate limitation, and

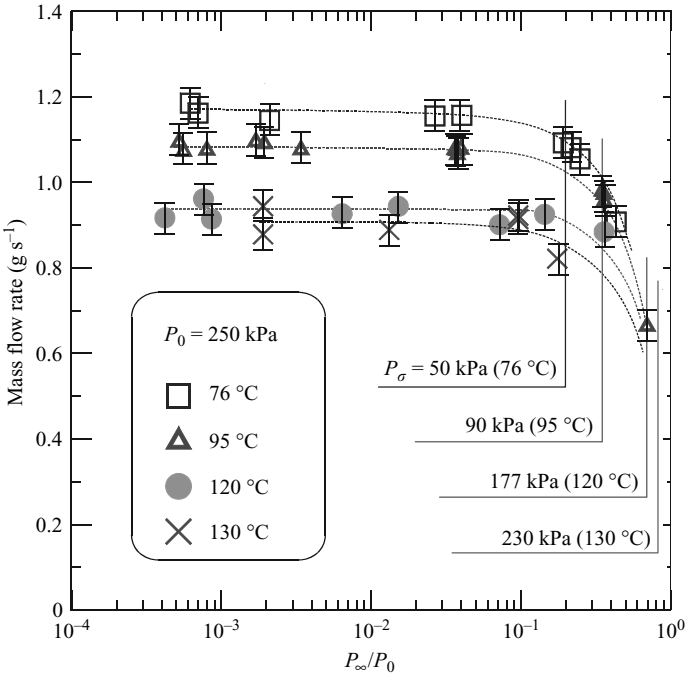

FIGURE 10. Measured mass flow rate as a function of the backpressure to injection pressure ratio for four different injection temperature and injection pressure equals to 250 kPa.

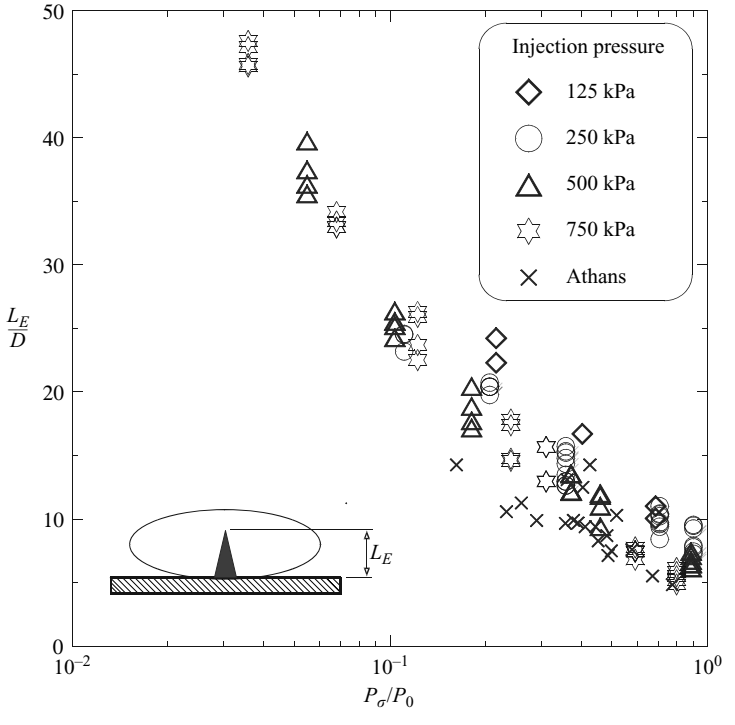

FIGURE 11. Ratio between the extinction length L_E to nozzle diameter D as a function of the ratio of saturation P_σ to injection pressure P_0.

P_0 ± 1.8 (kPa)	T_0 ± 1.2 (°C)	P_∞ ± 0.06 (kPa)	$R_P = P_\sigma / P_\infty$ –	$\dot{m}$ $\pm 2\%$ (g s^{-1})	L_E ± 0.5 (mm)
257.2	56.3	0.49	55.8	1.2350	7.6
250.2	56.5	0.28	100.6	1.2168	7.2
249.0	56.9	0.08	352.0	1.2103	7.6
250.8	95.0	9.07	9.9	1.1208	3.9
250.9	94.6	9.27	9.6	1.1237	4.0
250.4	95.2	9.40	9.6	1.1198	3.9
250.5	94.7	9.93	8.9	1.1210	4.0
246.8	93.9	0.85	102.1	1.1194	4.7
250.0	94.4	0.49	181.6	1.1342	4.4
252.2	95.4	0.43	213.3	1.1412	4.2
251.4	95.2	0.20	450.8	1.1277	4.6
496.8	77.3	5.07	10.4	1.7163	7.8
501.9	76.2	0.93	54.2	1.7079	7.5
496.3	76.7	0.48	108.2	1.6955	8.1
497.6	76.9	0.11	474.8	1.6993	7.9
753.0	76.2	4.90	10.2	2.101	10.5
749.2	76.8	1.00	51.3	2.100	10.3
752.5	77.0	0.54	94.7	2.091	10.2
750.7	77.1	0.21	241.5	2.114	10.3

TABLE 2. Liquid core extinction length, L_E, for tests having several injection pressure and temperatures.

unchanging liquid core length. All of these phenomena are explained in the context of the present physical model.

In order to investigate whether internal nucleation was taking place, in which case the hypothesis of an intact metastable liquid core would not be applicable, the photographs taken from different experimental conditions were examined. First, it was noticeable that the issuing liquid jet was always regular in its cylindrical and axisymmetrical geometrical shape, from which it was possible to infer that if nucleation were taking place inside the nozzle, the jet geometry would probably behave randomly. Also, it would not be possible to measure any jet extinction length, since the jet would issue from the nozzle irregularly. Secondly, previous authors have also documented the existence of a metastable liquid core using different photographic techniques. Among those are Reitz (1990), Kurschat *et al.* (1992) and Athans (1995). Finally, experiments would not be reproducible with respect to the liquid core and a well-behaved extinction length seen in this work (L_E in tables 1 and 2) would not be expected.

4.2. *Shock waves*

In all tests where shock waves were visible, the jets were also choked as a limiting mass flow rate was achieved, independently of the backpressure, as already discussed (see also figure 10). Shock waves were mostly formed by closed shock structures surrounding the liquid core. Depending on the test temperature and pressure, the overall shock wave took an ellipsoid shape in some experiments and a spheroidal form in others. They were visible for R_P around and above 50 at test temperatures of 56 °C and 76 °C. For higher temperatures (131 °C and 178 °C), shock waves could be distinguished for R_P of nearly 100 and above. An important consequence of constant

mass flow rate is that the metastable liquid pressure at the exit section is also constant, according to (2). Another important results of these tests was that the liquid core was stable and regular, i.e. its extinction length and shape were the same, regardless of how much the backpressure had been reduced.

Tests at a given injection pressure and temperature for variable backpressure indicated that the overall shock-wave dimensions increased with decreasing backpressure, as seen from an inspection of the corresponding photographs. This also shows that the mean standing location of the shock-wave structure was a farther away from the nozzle exit as the backpressure was lowered. In order to roughly estimate the main dimensions of the shock-wave structure, we may associate characteristic radial, r_1, and axial, r_2, lengths as shown in figures 12 to 15. The experimental data presented in those graphs indicate that both of those characteristic lengths decrease with increasing backpressure. Figures 12 and 13 display results of tests with a constant injection pressure for several test temperatures. Temperature tended to have more influence at a higher injection pressure (figure 13) and was not significant for a low injection pressure (figure 12). In two other test series, the injection temperature was the constant parameter, as shown in figures 14 and 15 while the injection pressure took different values. Higher injection pressures yield a larger axial dimension, r_2. However, the radial length, r_1, is more sensitive to backpressure variation.

During the tests, the backpressure rose slightly as a non-negligible amount of test fluid vapour was accumulated in the low-pressure chamber because a typical test run lasted a few seconds. A low-time-constant pressure transducer was installed in the chamber to monitor the backpressure rise. As a second precaution, more than one still picture was taken sequentially for each test run for later visual analysis. For example, figure 16 shows test progress documented by photographs taken about 1 s apart for the test conditions indicated. The pressure transducer signal recorded that the backpressure rose from 0.05 kPa to 0.14 kPa. The 0.09 kPa backpressure increase had a non-negligible influence upon the overall shock-wave dimensions. The sequence of photographs shows that the shock wave shrank as the backpressure increased.

A final important issue is whether the phenomenon seen in the photographs is in facts a shock wave. In order to prove that the phenomena are shock waves, or a shock-wave structure, a sharp blade (shaving blade) was installed in the vicinity of the exit region of the jet where supersonic two-phase flow dominates. As seen in figure 17, the shock wave does not undergo any visible perturbation on the left-hand side, whereas on the right-hand-side a complex shock wave is formed upstream of the obstacle, as is typical in supersonic flows. In addition, a shock-wave reflection on the bottom wall is also visible. Therefore, this test proves that the phenomena seen are shock waves and supersonic flows are also present.

5. Physical modelling and solution

5.1. *Overall behaviour*

A physical model (Simões-Moreira *et al.* 2002; Angelo & Simões-Moreira 2004; Vieira & Simões-Moreira 2004) has been proposed that encompass the various compressible phenomena and the overall behaviour of a flashing liquid jet at the very low backpressure range examined here. Referring to the picture and schematics of figure 18, compressed liquid is initially at injection condition '(0)'. As the test liquid flows inside the nozzle, it undergoes first an internal expansion process '(0→1)', taking the test liquid into a metastable state '(1)' to the exit section if no nucleation takes place within the nozzle. As is usual for liquids, the internal expansion is nearly isothermal

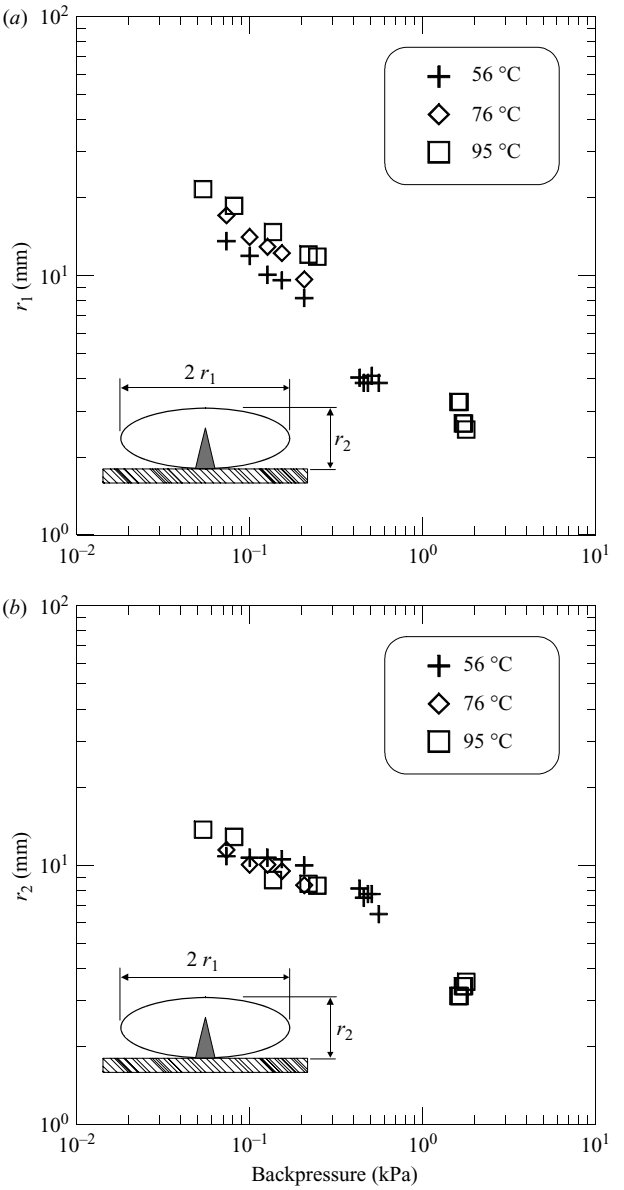

FIGURE 12. The representative lengths (*a*) r_1 and (*b*) r_2 are compared with run series where the injection pressure is 125 kPa.

and the incompressible hypothesis holds as a good approximation. By assumption, the metastable liquid state '(1)' is uniform and constant across the nozzle exit section and it remains at the same thermodynamic state '(1)' within the whole central liquid core. Next, experimental observations imply that a sudden phase transition '(1) → (2)' takes place on the central liquid core surface through an oblique evaporation wave, a phenomenon that has been studied by Simões-Moreira (2000). A phase-change process through evaporation waves is vigorous evaporation in which a metastable liquid is transformed into a high-speed two-phase flow in a discrete interface or flow

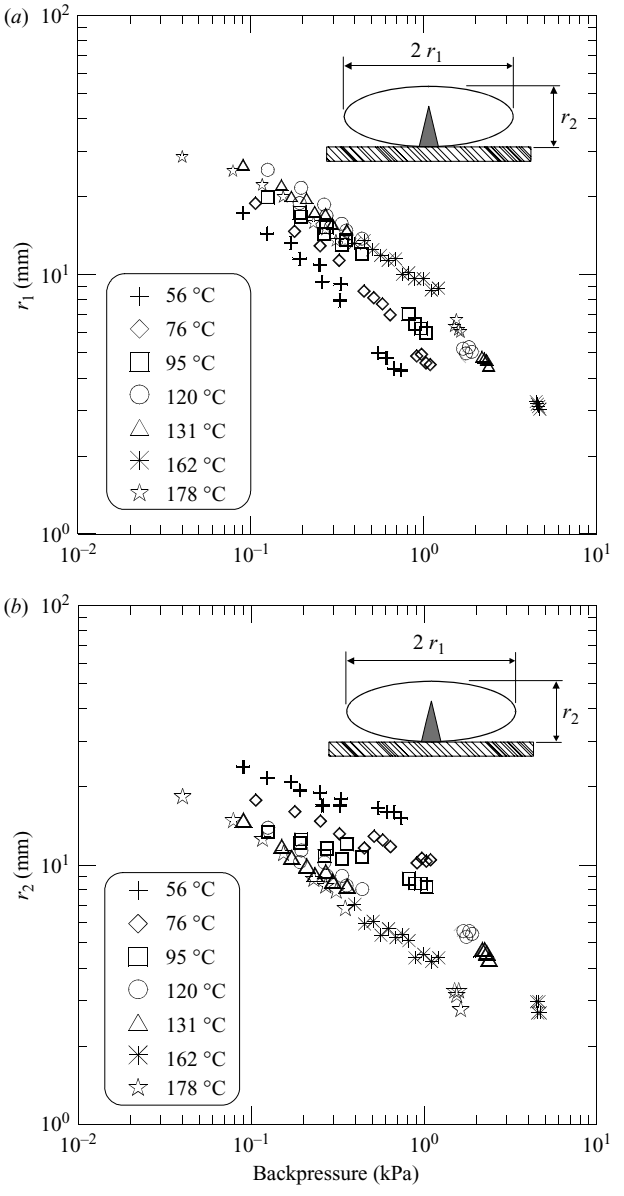

FIGURE 13. The representative lengths (*a*) r_1 and (*b*) r_2 are compared with run series where the injection pressure is 750 kPa.

discontinuity. The evaporation interface breaks the flow field up into two distinct regions: the upstream metastable liquid and the downstream two-phase flow. The solution of the conservation laws of mass, momentum and energy shows that fluid pressure, density and, of course, temperature decrease as a consequence of the sudden evaporation process (Simões-Moreira 2000) as the flow is accelerated because of the abrupt evaporation. At extreme conditions, such as those tested here, the normal velocity component of the two-phase flow is sonic compared to the evaporation wave front frame in a condition known as the Chapman–Jouguet point. Next, the

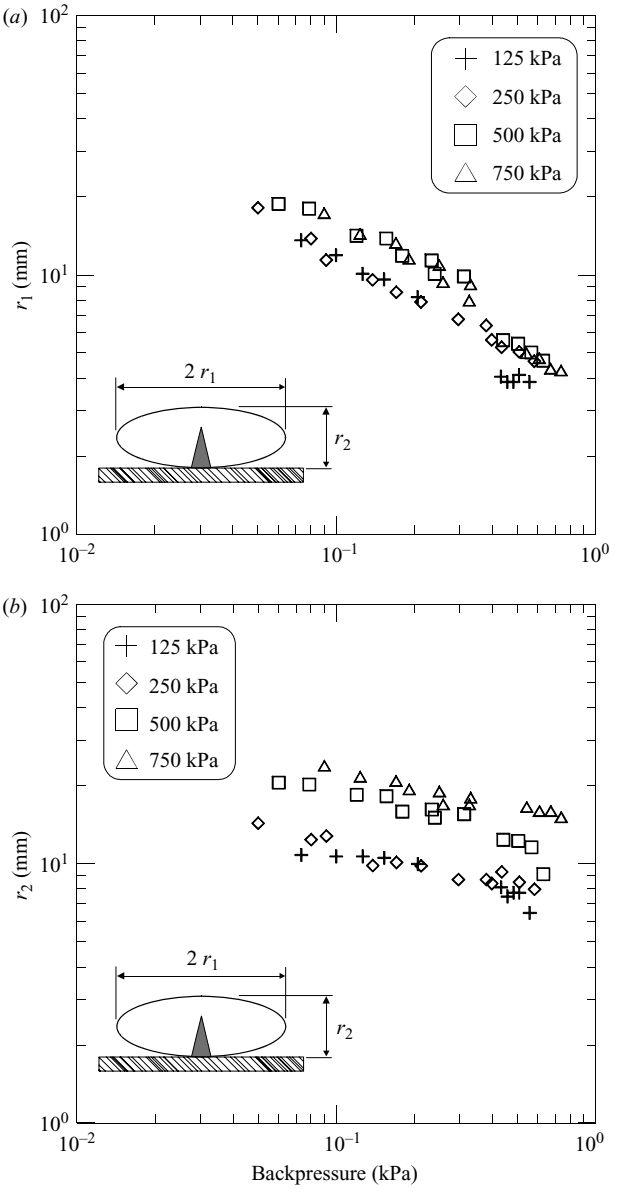

FIGURE 14. The representative lengths (*a*) r_1 and (*b*) r_2 are compared with run series where the injection temperature is 56 °C.

newly formed downstream sonic two-phase flow expands freely from the oblique evaporation wave to increasing supersonic velocities, which comprises the expansion process '(2) → (3)' in figure 18. Finally, the supersonic expansion process comes to an end through the formation of a regular compression shock wave '(3 → 4)' to match the fluid pressure with the backpressure in the far field, as is usual in compressible flow. All processes and thermodynamic states are also shown in the pressure-specific volume plane in figure 18. Other details of the thermodynamic model can be found in Angelo & Simões-Moreira (2004).

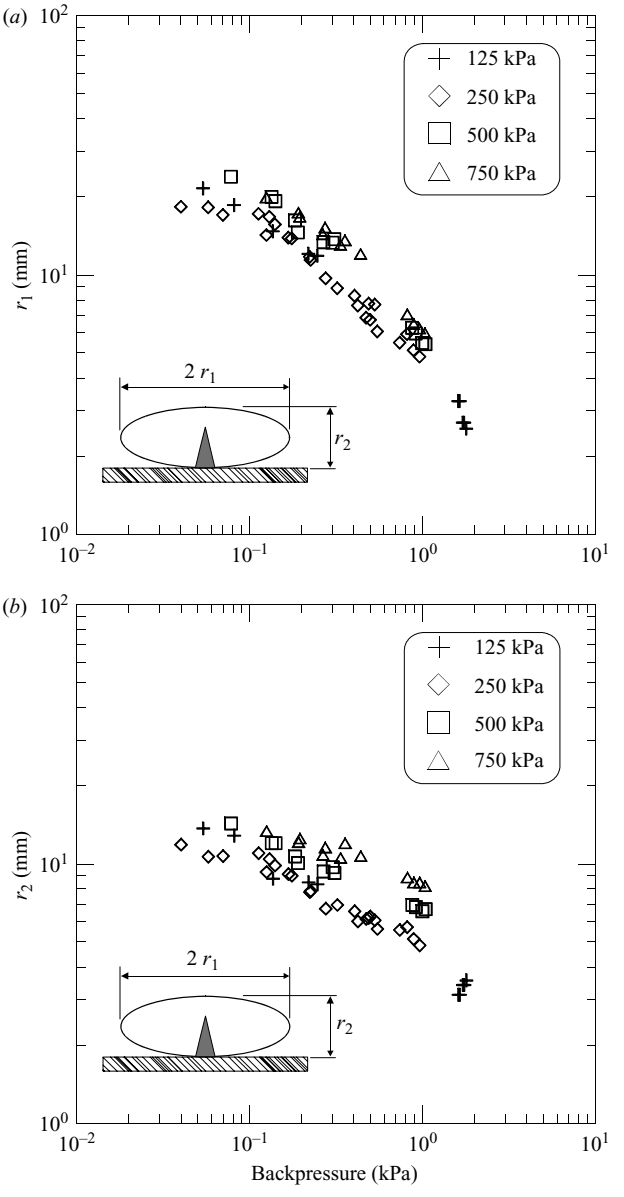

FIGURE 15. The representative lengths (*a*) r_1 and (*b*) r_2 are compared with run series where the injection temperature is 95 °C.

5.2. *Oblique evaporation wave jump equations*

To calculate the jump in thermodynamic properties and other flow parameters across the metastable liquid two-phase oblique interface '(1) → (2)', the laws of conservation of mass, momentum and energy must be solved. The main assumption is that there exist uniform thermodynamic properties within a phase domain, which means that the downstream state '(2)' is at thermodynamic equilibrium (thermal and mechanical), and that the evaporation process is at steady state. Therefore, the one-dimensional

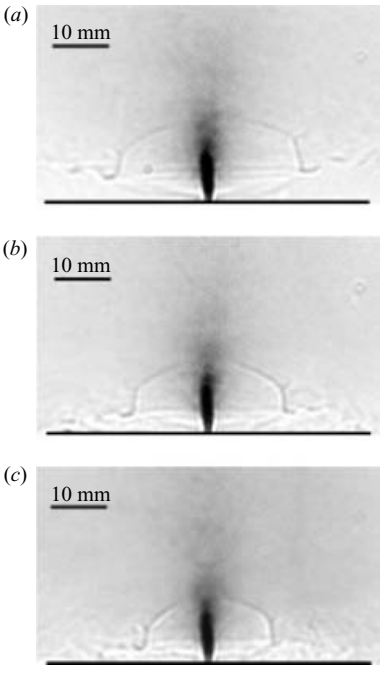

FIGURE 16. Schlieren photographs from a single liquid jet 1 s apart from each other. Initial pressure and temperature were 249.0 kPa and 56.9 °C, $R_P = 500$. Backpressures were (*a*) 0.05, (*b*) 0.09 and (*c*) 0.14. Shock wave structure 'shrinks down' as backpressure increases.

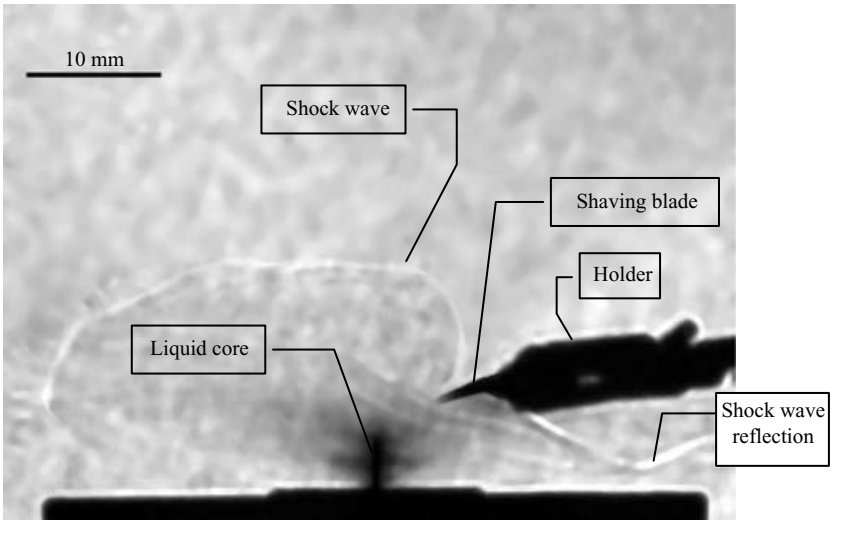

FIGURE 17. Shock waves around an obstacle (shaving blade) indicating the presence of a supersonic flow.

mass, momentum and energy conservation equations are, respectively,

$$[J] = 0, \tag{3}$$

$$[P + WJ] = 0, \tag{4}$$

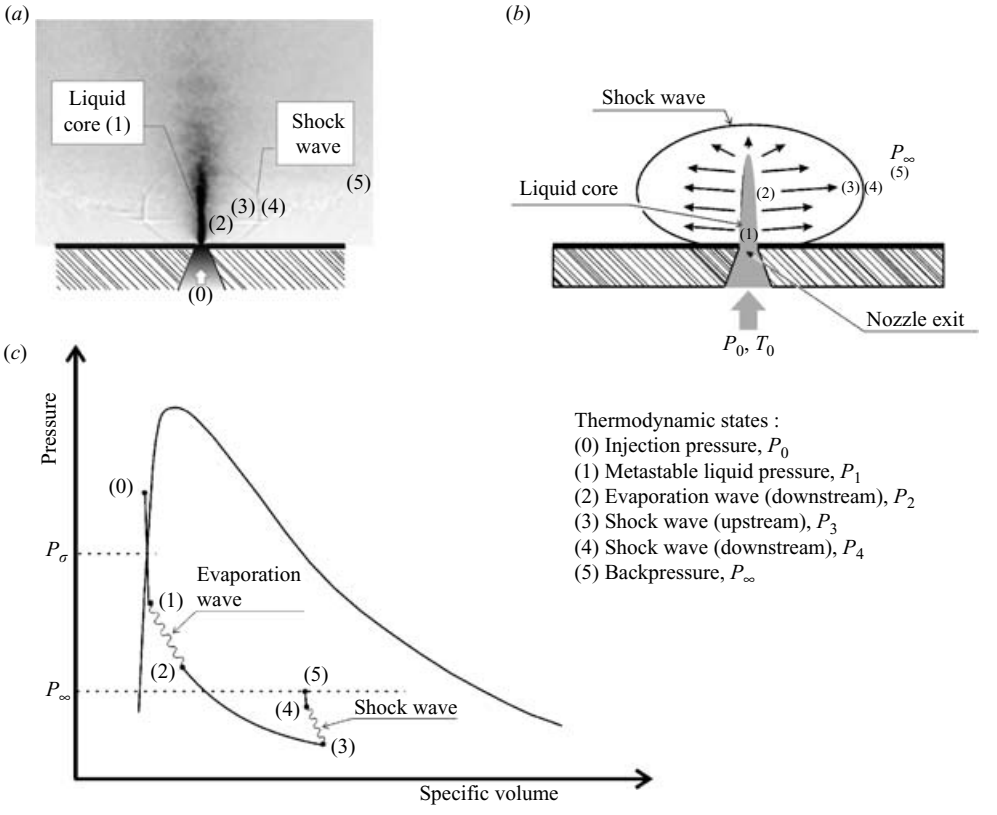

FIGURE 18. General behaviour of a highly expanded liquid jet: (*a*) the jet, stressing the main thermodynamic states, which are also indicate in (*b*) pressure-specific volume plane, and (*c*) schematic of upstream and downstream velocities and angles for an oblique evaporation wave.

$$\left[h + \frac{W^2}{2}\right] = 0, \tag{5}$$

where the square brackets indicate a jump between an upstream, '1', and a downstream, '(2)', parameter or property, that is, $[f] = f_2 - f_1$. J is the normal *superficial* mass flow rate across the oblique evaporation wave or front, W is the normal relative velocity, h is the specific enthalpy, and P is the pressure. Previous studies and analysis (Simões-Moreira & Shepherd 1999) have shown that for a given upstream metastable liquid state '(1)', there exists a corresponding singular solution for low downstream pressures '(2)', below some threshold value. This solution is the Chapman–Jouguet (C-J) condition and the corresponding normal superficial mass flow rate is J_{CJ}. At the C-J condition, the two-phase normal velocity (W_2) is sonic compared to the oblique evaporation wave front. The oblique evaporation wave makes an angle β with the liquid jet exit velocity u_1 whilst the downstream flow is deflected through an angle θ (see also figure 19). The wave angle β can be found according to:

$$\sin\,\beta = \frac{J_{CJ}}{J_N} = \frac{\pi W_2 D^2}{4 v_2 \dot{m}}, \tag{6}$$

where J_N is the superficial mass flow rate referred to the nozzle exit cross-section area, and v_2 is the downstream specific volume. The assumption leading to (6) is that

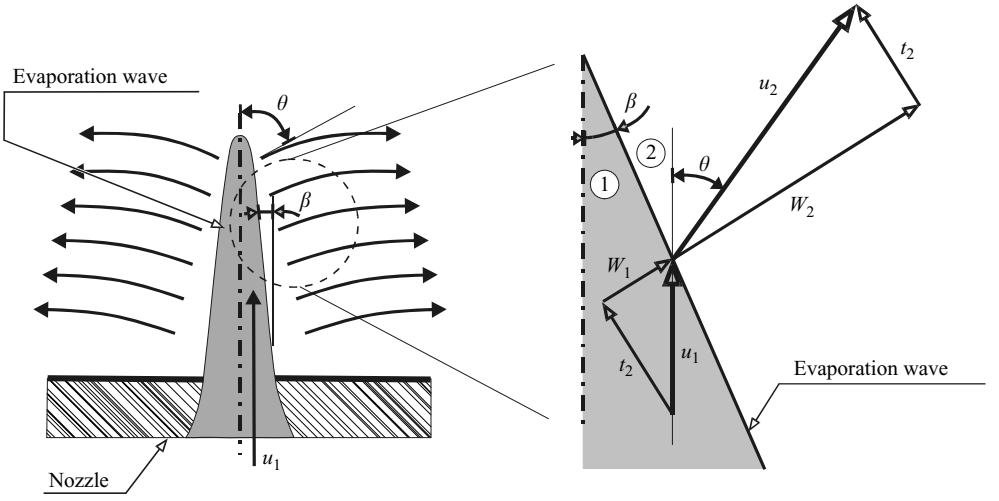

FIGURE 19. Velocity diagrams, turning angle θ, wave angle β, oblique evaporation wave, and the cone of evaporation.

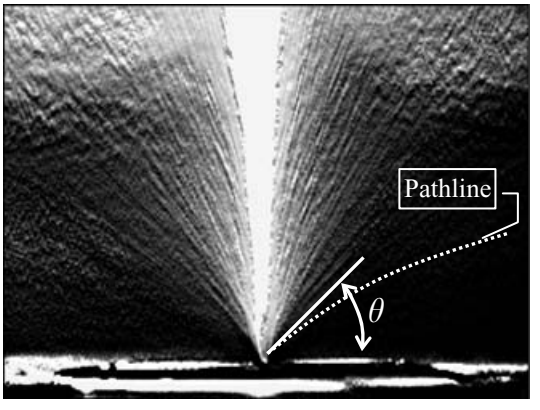

FIGURE 20. Droplets expanding from the liquid core. An imaginary trajectory of the fluid is represented. The image was filtered and processed mathematically to highlight the droplets ($P_0 = 752.0\,\text{kPa}$, $T_0 = 56.4\,^\circ\text{C}$, and $P_\infty = 0.21\,\text{kPa}$)

the metastable liquid core has a conical shape (the 'cone of evaporation') having the exit nozzle diameter, D, as base (figure 19). Thermodynamic properties are constant and uniform within the cone of evaporation.

Simões-Moreira (2000) discusses the trigonometric relationship between upstream and downstream velocities, thermodynamic properties, and wave and turning angles. The final expression relating all of the important parameters is given by

$$\tan\theta = \frac{\sin(2\beta)}{2\left(\sin^2\beta + \dfrac{1}{v_2/v_1 - 1}\right)}. \tag{7}$$

The assumption of an oblique evaporation wave is based on many experimental observations, from which the velocity diagram of figure 19 was constructed. Figure 20 shows the flow path turning. The fluid (actually, small droplets) bends away from the central liquid core. The picture analysis issue must be examined in more detail

P_0 (kPa)	T_0 (°C)	$\dot{m}$ ($g\,s^{-1}$)	P_1 (kPa)	P_2 (kPa)	T_2 (°C)	x_2 —	v_2 ($m^3\,kg^{-1}$)	W_2 ($m\,s^{-1}$)	J_{CJ} ($kg\,m^2\,s^{-1}$)	β (deg.)	L_E calc. (mm)	L_E meas. (mm)
122.1	56.4	0.8447	4.2	2.3	4.3	0.352	3.1772	78.3	24.6	0.1215	72.74	6.2
122.7	75.2	0.8340	6.6	3.5	12.2	0.436	2.6379	90.4	34.3	0.1726	51.21	4.2
123.5	94.8	0.8022	14.7	7.8	28.6	0.481	1.3863	97.8	70.5	0.3722	23.74	2.3
249.0	56.9	1.2103	9.4	5.5	21.1	0.251	1.0029	62.7	62.5	0.2164	40.84	7.4
251.8	76.6	1.1872	18.4	10.6	35.1	0.304	0.6634	72.2	108.9	0.3870	22.84	6.3
250.5	94.7	1.1210	39.4	23.4	54.6	0.311	0.3285	72.7	221.4	0.8389	10.53	4.3
249.6	120.2	0.9456	94.7	57.7	80.3	0.337	0.1555	76.2	490.3	2.2151	3.99	3.1
257.1	130.9	0.8102	140.8	88.5	94.4	0.324	0.1012	73.3	724.9	3.8163	2.31	2.9
501.6	56.6	1.7455	15.9	10.2	34.3	0.163	0.3694	46.0	124.7	0.3030	29.17	11.5
497.6	76.9	1.6993	30.6	19.4	49.6	0.209	0.2621	54.4	207.5	0.5216	16.94	7.8
503.4	95.4	1.6528	53.6	33.6	64.5	0.248	0.1881	61.6	327.7	0.8511	10.38	5.7
503.3	120.6	1.4822	131.8	88.7	94.4	0.233	0.0729	56.7	777.4	2.2685	3.89	3.9
500.0	131.0	1.3757	175.1	120.0	105.1	0.240	0.0571	57.0	997.8	3.1425	2.81	3.6
502.1	162.1	0.9286	342.8	234.0	131.7	0.316	0.0404	67.8	1680.0	7.8078	1.12	2.1
750.4	56.1	2.1471	21.7	16.4	45.3	0.084	0.1240	26.0	209.2	0.4150	21.29	14.4
752.5	77.0	2.0910	50.5	42.7	71.2	0.050	0.0320	16.2	508.1	1.0421	8.48	10.3
748.4	95.3	2.0112	89.9	78.9	90.4	0.046	0.0173	14.5	838.2	1.7994	4.91	7.6
753.2	121.1	1.8833	161.0	121.8	105.7	0.145	0.0347	37.8	1089.3	2.5189	3.51	5.0
749.6	131.9	1.7599	224.6	185.0	121.9	0.102	0.0173	27.6	1591.8	3.9481	2.23	4.4
749.2	161.8	1.3746	409.2	320.7	145.8	0.180	0.0178	41.9	2349.9	7.4709	1.18	2.3
751.6	178.1	0.9809	569.5	458.3	163.2	0.183	0.0131	41.3	3141.1	14.0041	0.62	1.7

TABLE 3. Oblique evaporation wave calculation results for several injection conditions.

because only droplets are visible, since the vapour phase leaves no traces that can be captured by this photographic technique alone without proper mathematical filtering. The photographic work of Athans (1995) also corroborates these findings.

More indirect evidence of the validity of the present physical modelling comes from measurements of the extinction length, L_E. By assumption, the cone of evaporation has a conical shape; therefore it is straightforward to show that

$$\tan\beta = \frac{D}{2L_E}. \tag{8}$$

Equation (8) is useful for estimating the wave angle, β, from the corresponding measured extinction length, L_E.

In table 3, a series of experimental results along with the calculated downstream properties are presented. The first three columns indicate the injection pressure and temperature, and the measured mass flow rate, respectively. The next column presents the corresponding metastable liquid pressure as calculated according to (2). The next set of five columns with magnitudes having a '2' index refer to the downstream solution of an oblique evaporation wave which can be obtained by solving the conservation equations (3) to (5) at the Chapman–Jouguet condition. The superficial mass flow rate at the C-J condition is also indicated. The wave angle is shown in the table, which was estimated from (6). The calculated extinction length is obtained from (8), using the estimated wave angle. The corresponding measured extinction length is shown in the last column. A comparison between measured and calculated extinction lengths is shown in figure 21. Uncertainty bars are also displayed. Uncertainties in the calculated extinction length are large as a function of the propagation of the

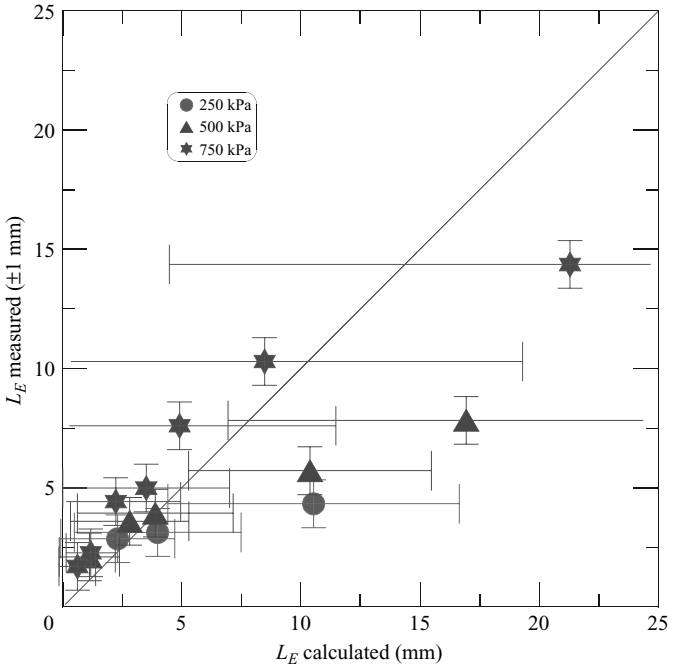

FIGURE 21. The curve compares the calculated L_E (meas.) with measured L_E (calc.). Data values are from table 3.

measured magnitudes. Nevertheless, the data tend to cluster around the central line, showing that the model anticipates well the measured extinction length. The model agrees better in the lower range.

6. Conclusions

Overall, three flashing regimes were observed, depending on the saturation pressure to backpressure ratio (R_P). For R_P around 1, a continuous liquid jet broken by sporadic nucleation was seen. As R_P increased, nucleation sites alongside the liquid jet were visible. For instance, for R_P around 2, the liquid jet was completely fragmented. On the very low backpressure regime, for R_P larger than around 50, some experiments have shown the presence of shock waves. Most of the experiments concentrated in the high R_P range, i.e. low backpressures.

A choking or limiting mass flow rate behaviour was also noticed. In tests at constant injection pressure and temperature, the mass flow rate increased as the backpressure decreased, as usual, down to a certain value. If the backpressure decreased below that value, the mass flow rate became insensitive to any further backpressure reduction, i.e. a maximum mass flow rate had been achieved, giving rise to a choking condition. The limiting mass flow rate value itself depended on the initial injection pressure and temperature. Another important finding was that a regular liquid core always formed. Its length remained nearly constant and insensitive to any further backpressure lowering beyond that choking point. Clearly, if random nucleation were taking place, the liquid core shape would be erratic and irregular, which is contrary to our experimental evidence.

Special photographic techniques were important for capturing the compressible phenomena associated with iso-octane flashing liquid jets issuing from small nozzles into a very low pressure chamber, for example, the shock waves. The associated shock waves formed had larger overall dimensions for lower backpressures. Also, a characteristic axial dimension of a shock-wave structure was larger for higher injection pressure and temperature. Schlieren photographs show that at extreme low backpressures, a liquid jet exits the nozzle without any perceptible nucleation site, forming the small liquid core, the so-called metastable liquid core. A vigorous evaporation took place on the surface of that liquid core. The schlieren photographic technique also allowed the authors to distinguish a complex shock-wave formation enveloping the liquid core. The many experiments carried out at different conditions in addition to a set of three photographs taken for each experiment, along with the constancy of both the mass flow rate and the injection pressure, clearly indicate that the tests were at a steady-state condition.

Those experimental observations agreed with previous work and established the groundwork for a physical modelling to explain all the observed phenomena. In the present modelling, the liquid exits the nozzle reaching a metastable condition, which can be calculated by using the incompressible orifice equation along with the discharge coefficient (2). Next, the metastable liquid undergoes a sudden phase transition through an oblique evaporation wave which comprises the surface of the liquid core which has been approximated by a geometrical cone, the 'cone of evaporation'. The present simplification comes from assuming that the thermodynamic state of the liquid within the liquid core is uniform and constant throughout the whole region having the same properties as the metastable liquid issuing from the nozzle, which leads to a uniform rate of evaporation. At extreme conditions (low backpressures), the strong phase-change process is limited by a maximum mass flow rate condition known as the Chapman–Jouguet point in analogy to a deflagration wave in a combusting gas. The Chapman–Jouguet (C-J) condition elucidates the choking phenomenon noticed in the experiments and, also, explains the jump in properties as the liquid evaporates within the evaporating phase-change front. The conservation jump equations were established for the interface two-phase flow and metastable liquid, i.e. the lateral area of the cone of evaporation which has been known as an oblique evaporation wave. By following the C-J theory, the relative normal is sonic compared to the oblique evaporation wave. That sonic flow expands further to higher Mach numbers to eventually form a complex strong regular compression shock wave. The shock-wave structure surrounds the liquid core and brings the high-speed two-phase flow to a low velocity to match the backpressure in the far field.

The authors thank FAPESP and CNPq, respectively, for personal support. This project was supported by FAPESP (proc. 2000/08302-6).

REFERENCES

Angelo, E. & Simões-Moreira, J. R. 2004 Liquid jets expanding into a low-pressure environment – numerical solution. *Third Intl Symposium of Two-Phase Flow Modeling and Experimentation*, AP-8, *Pisa, Italy, 22–24 Sept*.

Athans, R. E. 1995 The rapid expansion of near-critical retrograde fluid. PhD Thesis, Rensselaer Polytechnic Institute, NY, USA.

Kurschat, Th., Chaves, H. & Meier, G. E. A. 1992 Complete adiabatic evaporation of highly superheated jets. *J. Fluid Mech.* **236**, 43–58.

Lee, B. I. & Kesler, M. G. 1975 A generalized thermodynamic correlation based on three-parameter corresponding states. *AIChE J.* **21**, 510–527.

Lienhard, J. H. & Day, J. B. 1970 The breakup of superheated liquid jets. *Trans. ASME D: J. Basic Engng* **92**, 515–521.

Oza, R. D. & Sinnamon, J. F. 1983 An experimental and analytical study of flash-boiling fuel injection. *Intl Congress & Exposition, Society of Automotive Engineers*, paper # 830590, *Detroit, Michigan, USA*.

Reitz, R. D. 1990 A photographic study of flash-boiling atomization. *Aerosol Sci. Techn.* **12**, 561–569.

Simões-Moreira, J. R. 2000 Oblique evaporation waves. *Shock Waves – An International Journal on Shock Waves, Detonations and Explosions*, vol. 10, No. 4, pp. 229–234.

Simões-Moreira, J. R. & Shepherd, J. E. 1999 Evaporation waves in superheated dodecane. *J. Fluid Mech.* **382**, 63–68.

Simões-Moreira, J. R., Vieira, M. M. & Angelo, E. 2002 Highly expanded flashing liquid jets. *J. Thermophys. Heat Transfer*, **16**, 415–424.

Vieira, M. M. 2005 Estudo experimental da evaporação de jatos de isso-octano superaquecidos. Doctoral Thesis, Escola Politécnica da Universidade de São Paulo, Brazil (in Portuguese).

Vieira, M. M. & Simões-Moreira, J. R. 2004 Liquid jets expanding into a low-pressure environment – experimental results. *Third Intl Symposium on Two-Phase Flow Modelling and Experimentation*, AP-8, Pisa, Italy, 22–24 Sept.

Vieira, M. M. & Simões-Moreira, J. R. 2006 A photographic study of flashing liquid jets. *6th Intl Conference on Boiling Heat Transfer*, Spoleto, Italy, 7–12 May.